

Use of long-period surface waves for rapid determination of earthquake-source parameters

Hiroo Kanamori and Jeffrey W. Given

Seismological Laboratory, California Institute of Technology, Pasadena, CA 91125 (U.S.A.)

(Received January 7, 1981; accepted for publication February 26, 1981)

Kanamori, H. and Given, J.W., 1981. Use of long-period surface waves for rapid determination of earthquake-source parameters. *Phys. Earth Planet. Inter.*, 27: 8–31.

A method for rapid retrieval of earthquake-source parameters from long-period surface waves is developed. With this method, the fault geometry and seismic moment can be determined immediately after the surface wave records have been retrieved. Hence, it may be utilized for warning of tsunamis in real time. The surface wave spectra are inverted to produce either a seismic moment tensor (linear) or a fault model (nonlinear). The method has been tested by using the IDA (International Deployment of Accelerographs) records. With these records the method works well for the events larger than $M_s = 6$, and is useful for investigating the nature of slow earthquakes.

For events deeper than 30 km, all of the five moment tensor elements can be determined. For very shallow events ($d \leq 30$ km) the inversion becomes ill-conditioned and two of the five source moment tensor elements become unresolvable. This difficulty is circumvented by a two-step inversion. In the first step, the unresolvable elements are constrained to be zero to yield a first approximation. In the second step, additional geological and geophysical data are incorporated to improve the first approximation. The effect of the source finiteness is also included.

1. Introduction

The number of digital seismograph stations has recently increased dramatically, and high-quality digital seismograms are now widely available. This paper describes a method for the determination of earthquake source parameters by using long-period surface waves obtained from these digital stations, particularly the IDA (International Deployment of Accelerographs; Agnew et al., 1976) stations.

Various methods have been developed for different seismological investigations. Seismic body waves, both the first motion and the wave forms, have been extensively used for the determination of the source geometry, the depth and the seismic moment at relatively short periods. Seismic surface waves and free oscillations have been used for the determination of long-period source parameters.

Among the most recent works of this type are those by Masters and Gilbert (1979) and Dziewon-ski et al. (1981).

The primary objectives of the present study are as follows:

- (1) to develop a very quick method which can be used for real-time tsunami warning purposes;
- (2) to determine the long-period seismic moment (either scalar or tensor) of events as small as $M_s = 6$.

Tsunamis are primarily caused by earthquake-generated deformations of the sea bottom with time scales up to several hundred seconds. Therefore, to evaluate the tsunami potential of an earthquake, it is most important to determine accurately the size and the mechanism of the earthquake at long periods. If these earthquake parameters are to be used in real-time warning systems,

the source mechanism has to be determined within at least one hour of the earthquake origin time. The method described here would meet this requirement.

The source spectra of earthquakes vary significantly from event to event. Some earthquakes have a disproportionately large amount of energy at the long-period end of the spectrum, whereas others have enhanced short-period spectra. Certain earthquakes are often called tsunami earthquakes or slow earthquakes because of their anomalously large ratio of long-period to short-period radiation. Whether or not these anomalous earthquakes occur only at certain special plate boundaries has an important bearing on the mechanical property of the plate boundary and the nature of the plate motion there. In the past this study could not be made for small events because of the lack of adequate long-period instruments. Therefore, the sample size of the data was too limited to investigate the possible regional variation. The availability of high-quality long-period data would significantly expand the data base if an appropriate method were developed. Although the method described in this paper has been developed to achieve these specific goals, it can also be used for more general purposes and would be complementary to the various existing methods.

The theories of excitation (Satô et al., 1962; Haskell, 1963, 1964; Harkrider, 1964; Ben-Menahem and Harkrider, 1964; Saito, 1967; Ben-Menahem et al., 1970; Gilbert, 1970) and of inversion (Aki, 1966; Dziewonski and Gilbert, 1974; Gilbert and Dziewonski, 1975; Gilbert and Buland, 1976; Patton, 1980; Aki and Richards, 1980) of surface waves and free oscillations have been thoroughly developed. The present paper makes use of the results of these developments and is similar, in spirit, to the paper by Ben-Menahem et al. (1970). The primary emphasis here is on some practical problems in applying these theories to real data.

2. Method

In this section we briefly describe the method for spheroidal oscillations or Rayleigh waves by

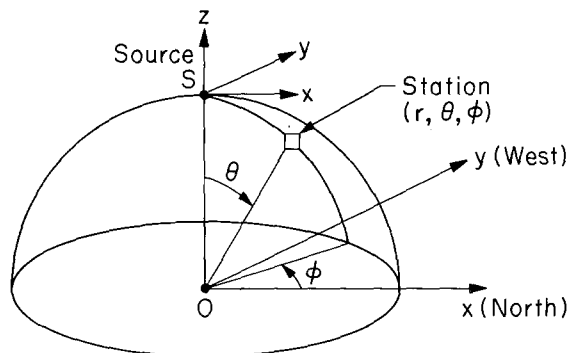


Fig. 1. Definition of the coordinates.

using the notation of Kanamori and Cipar (1974) and Kanamori and Stewart (1976). We use either a seismic-moment tensor source (Gilbert, 1970) or a double-couple (fault) source. First we describe the method for a moment tensor source.

We take a spherical coordinate system (r, θ, ϕ) with the origin at the center of a spherically symmetric, non-rotating Earth model. A point source defined by a moment tensor $(M_{xx}, M_{yy}, M_{zz}, M_{xy}, M_{xz}, M_{yz})$ is placed at $r = r_s$ on the polar axis. The moment tensor is defined with respect to a Cartesian coordinate system (x, y, z) with the origin at the source, and the x , y and z axes are in the northern, western and upward vertical directions (Fig. 1). Then, by the notation of Kanamori and Cipar (1974), Okal (1978) and Okal and Geller (1979), the vertical component of spheroidal oscillations at point P (r, θ, ϕ) due to a step-function point source is given by

$$\begin{aligned}
 u_z(\mathbf{r}, t) = \sum_l y_l(r) \cos \omega_l t \left\{ \right. & \left. -K_2 P_l^2 M_{xy} \sin 2\phi \right. \\
 & \left. + \frac{1}{2} K_2 P_l^2 (M_{yy} - M_{xx}) \cos 2\phi \right] \\
 & + \left(-K_1 P_l^1 M_{yz} \sin \phi \right. \\
 & \left. - K_1 P_l^1 M_{xz} \cos \phi \right) + \left[\frac{1}{3} (K_0 + N_0) P_l^0 M_{zz} \right. \\
 & \left. + \frac{1}{6} (2N_0 - K_0) P_l^0 (M_{xx} + M_{yy}) \right] \left. \right\} \quad (1)
 \end{aligned}$$

where the azimuthal angle ϕ is measured counterclockwise from the x axis. The excitation functions

K_0 , K_1 and K_2 are given by Kanamori and Cipar (1974) and N_0 is given by Okal (1978). By taking the asymptotic expansion of (1), we obtain for the vertical component of Rayleigh waves

$$u_r(\mathbf{r}, t) = \frac{1}{2\pi} \int_{-\infty}^{+\infty} \hat{C}_R(\omega) \exp(i\omega t) d\omega$$

where

$$\begin{aligned} \hat{C}_R(\omega) = & \frac{1}{(\sin \theta)^{1/2}} \exp\left(\frac{1}{4}\pi i\right) \\ & \exp\left(-\frac{i\omega a\theta'}{C}\right) \exp\left(\frac{1}{2}m\pi i\right) \\ & \left\{ -P_R^{(1)} \left[M_{xy} \sin 2\phi - \frac{1}{2}(M_{yy} - M_{xx}) \cos 2\phi \right] \right. \\ & + \frac{1}{3}(S_R^{(1)} + N_R^{(1)})M_{zz} \\ & + \frac{1}{6}(2N_R^{(1)} - S_R^{(1)})(M_{xx} + M_{yy}) \\ & \left. + iQ_R^{(1)}(M_{yz} \sin \phi + M_{xz} \cos \phi) \right\} \quad (2) \end{aligned}$$

$P_R^{(1)}$, $S_R^{(1)}$ and $Q_R^{(1)}$ are the excitation functions given by Kanamori and Stewart (1976), and

$$N_R^{(1)} = (\pi/2l)^{1/2}(a/U)N_0$$

where l is the order number, a the radius of the Earth, and U the group velocity; m is the number of the polar and antipolar passages, and θ' (rad) is the propagation distance

$$\theta' = 2\pi[(m+1)/2] + (-1)^m\theta$$

where $[]$ represents the largest integer equal to, or less than, the argument. Expression 2 is equivalent to that derived by McCowan (1976) and Mendiguren (1977).

The first, second, third and fourth factors on the right-hand side of (2) represent the geometrical spreading, the source phase, the phase shift during propagation and the polar phase shift respectively. We can analyze the data either as modes (free oscillations) by using (1), or as surface waves by using (2). Dziewonski and Gilbert (1974), Gilbert and Dziewonski (1975), Gilbert and Buland (1976) and Masters and Gilbert (1979) describe a complete procedure for retrieving source parameters

from modal data. Here we use propagating waves and use (2) for the analysis.

As discussed by Mendiguren (1977), since the data from the fundamental mode alone cannot resolve the isotropic component, we assume that

$$M_{xx} + M_{yy} + M_{zz} = 0 \quad (3)$$

We also assume the earthquake to be a point source that varies as a step function in time. This assumption will be removed later. Let $U_r(\mathbf{r}, t)$ be a Rayleigh wave seismogram (vertical component) recorded at station $P(\mathbf{r})$, and $\hat{U}_r(\mathbf{r}, \omega)$ its spectrum. Then $\hat{C}_R(\omega)$ in (2) can be obtained from $\hat{U}_r(\mathbf{r}, \omega)$ by correcting for the instrument response and the attenuation along the path

$$\hat{C}_R(\omega) = \hat{U}_r(\mathbf{r}, \omega) \exp(\omega a\theta'/2QU)/\hat{I}(\omega) \quad (4)$$

where \hat{I} is the complex instrument response and Q is the effective Q along the path. Substituting (3) and (4) into (2), we have

$$\begin{aligned} \hat{V}_r(\mathbf{r}, \omega) = & \left\{ -P_R^{(1)} \left[M_{xy} \sin 2\phi \right. \right. \\ & \left. \left. - \frac{1}{2}(M_{yy} - M_{xx}) \cos 2\phi \right] \right. \\ & \left. - \frac{1}{2}S_R^{(1)}(M_{yy} + M_{xx}) \right. \\ & \left. + iQ_R^{(1)}(M_{yz} \sin \phi + M_{xz} \cos \phi) \right\} \quad (5) \end{aligned}$$

where

$$\begin{aligned} \hat{V}_r(\mathbf{r}, \omega) = & (\sin \theta)^{1/2} \hat{U}_r(\mathbf{r}, \omega) \exp\left(\frac{\omega a\theta'}{2QU}\right) \\ & \exp\left(\frac{i\omega a\theta'}{C}\right) \exp\left(-\frac{1}{4}\pi i\right) \\ & \exp\left(-\frac{1}{2}m\pi i\right)/\hat{I}(\omega) \quad (6) \end{aligned}$$

If the phase velocity $C(\omega)$ is known for the path, $\hat{V}_r(\mathbf{r}, \omega)$ can be computed from the observed spectrum $\hat{U}_r(\mathbf{r}, \omega)$ by using (6).

From Rayleigh wave records at N stations P_1, P_2, \dots, P_N we obtain $\hat{V}_r(\mathbf{r}_k, \omega)$ ($k=1, \dots, N$), and (5) can be written as

$$\mathbf{AM} = \mathbf{V} \quad (7)$$

where

$$A = \begin{pmatrix} -P_R^{(1)} \sin 2\phi_1 & \frac{1}{2}P_R^{(1)} \cos 2\phi_1 & -\frac{1}{2}S_R^{(1)} & 0 & 0 \\ 0 & 0 & 0 & Q_R^{(1)} \sin \phi_1 & Q_R^{(1)} \cos \phi_1 \\ -P_R^{(1)} \sin 2\phi_2 & \frac{1}{2}P_R^{(1)} \cos 2\phi_2 & -\frac{1}{2}S_R^{(1)} & 0 & 0 \\ 0 & 0 & 0 & Q_R^{(1)} \sin \phi_2 & Q_R^{(1)} \cos \phi_2 \\ \vdots & \vdots & \vdots & \vdots & \vdots \\ -P_R^{(1)} \sin 2\phi_N & \frac{1}{2}P_R^{(1)} \cos 2\phi_N & -\frac{1}{2}S_R^{(1)} & 0 & 0 \\ 0 & 0 & 0 & Q_R^{(1)} \sin \phi_N & Q_R^{(1)} \cos \phi_N \end{pmatrix}$$

$$\mathbf{M} = \begin{pmatrix} M_{xy} \\ M_{yy} - M_{xx} \\ M_{yy} + M_{xx} \\ M_{yz} \\ M_{xz} \end{pmatrix}$$

$$\mathbf{V} = \begin{pmatrix} \text{Re } \hat{V}_r(\mathbf{r}_1, \omega) \\ \text{Im } \hat{V}_r(\mathbf{r}_1, \omega) \\ \text{Re } \hat{V}_r(\mathbf{r}_2, \omega) \\ \text{Im } \hat{V}_r(\mathbf{r}_2, \omega) \\ \vdots \\ \text{Re } \hat{V}_r(\mathbf{r}_N, \omega) \\ \text{Im } \hat{V}_r(\mathbf{r}_N, \omega) \end{pmatrix}$$

Thus, if the records are obtained at three or more stations, and if the matrix $A^T A$ is nonsingular, (5) can be solved for \mathbf{M} by the method of least squares.

Once the components M_{xx} , M_{yy} , etc. are determined, the eigenvalues λ_1 , λ_2 , λ_3 and the corresponding eigenvectors, \mathbf{v}_1 , \mathbf{v}_2 , \mathbf{v}_3 of the symmetric matrix

$$\begin{pmatrix} M_{xx} & M_{xy} & M_{xz} \\ M_{xy} & M_{yy} & M_{yz} \\ M_{xz} & M_{yz} & M_{zz} \end{pmatrix} \quad (8)$$

can be computed and the matrix diagonalized into

$$\begin{pmatrix} \lambda_1 & 0 & 0 \\ 0 & \lambda_2 & 0 \\ 0 & 0 & \lambda_3 \end{pmatrix} \quad (9)$$

Since the isotropic component is assumed to be zero, $\lambda_1 + \lambda_2 + \lambda_3 = 0$.

The eigenvectors \mathbf{v}_1 , \mathbf{v}_2 and \mathbf{v}_3 define the orientations of the principal stress axes. When the intermediate stress is zero, the moment tensor represents one double couple. When the intermediate stress is nonzero, it can be decomposed into one double couple and a compensated linear dipole (Knopoff and Randall, 1970), or a pair of orthogonal double couples. Here, following Gilbert (1981), we decompose the moment tensor into two double couples, the major and the minor. For example, if $|\lambda_1| \geq |\lambda_2| \geq |\lambda_3|$, the major double couple is defined by

$$\begin{pmatrix} \lambda_1 & 0 & 0 \\ 0 & -\lambda_1 & 0 \\ 0 & 0 & 0 \end{pmatrix} \quad (10)$$

and the minor double couple by

$$\begin{pmatrix} 0 & 0 & 0 \\ 0 & -\lambda_3 & 0 \\ 0 & 0 & \lambda_3 \end{pmatrix} \quad (11)$$

The standard fault parameters such as the strike, dip and slip angle for the individual double couples can be computed from the direction cosines of the eigenvectors. Useful relations for this transformation have been presented by Jarosch and Aboodi (1970).

For a double-couple (fault) source, we use eq. A-8 of Kanamori and Stewart (1976) and replace (5) by

$$\hat{V}_r(\mathbf{r}, \omega) = M_0 (s_R S_R^{(1)} + p_R P_R^{(1)} + i q_R Q_R^{(1)}) \quad (12)$$

where s_R , p_R and q_R are determined from the fault parameters δ (dip, angle), λ (slip angle) and ϕ_f (strike) defined by Fig. A-1 of Kanamori and Stewart (1976); M_0 is the scalar seismic moment. (In this case, there are four unknowns ($M_0, \delta, \lambda, \phi_f$) in contrast to the five unknowns for the moment tensor source. Since (12) is nonlinear with respect to the four unknowns, a first approximation is required to invert (12) by the method of nonlinear least squares.

Similar relations can be derived for torsional oscillations and Love waves. Using the notation of Kanamori and Cipar (1974), we obtain an expression for the transverse component of torsional oscillations at point \hat{P} (r, θ, ϕ) due to a point moment tensor source that varies as a step function in time

$$u_\phi(\mathbf{r}, t) = \sum_l y_l(r) \cos \omega_l t \left(\frac{1}{2} L_2 \frac{dP_l^2}{d\theta} (M_{xx} - M_{yy}) \sin 2\phi - L_2 \frac{dP_l^2}{d\theta} M_{xy} \cos 2\phi + L_1 \frac{dP_l^1}{d\theta} M_{xz} \sin \phi - L_1 \frac{dP_l^1}{d\theta} M_{yz} \cos \phi \right) \quad (13)$$

By using the asymptotic expansion of the spherical harmonics, for Love waves we have

$$\hat{V}_\phi(\mathbf{r}, \omega) = P_L^{(1)} \left[\frac{1}{2} (M_{xx} - M_{yy}) \sin 2\phi - M_{xy} \cos 2\phi \right] + iQ_L^{(1)} \left[-M_{xz} \sin \phi + M_{yz} \cos \phi \right] \quad (14)$$

where

$$\hat{V}_\phi(\mathbf{r}, \omega) = (\sin \theta)^{1/2} \hat{U}_\phi(\mathbf{r}, \omega) \exp\left(\frac{\omega a \theta'}{2QU}\right) \exp\left(\frac{i\omega a \theta'}{C}\right) \exp\left(\frac{1}{4}\pi i\right) \exp\left(-\frac{1}{2}m\pi i\right) / \hat{I}(\omega) \quad (15)$$

Here, $\hat{U}_\phi(\mathbf{r}, \omega)$ is the spectrum of the transverse component of the observed seismogram of Love waves. Equation 15 corresponds to (5) for Rayleigh waves.

For a double-couple (fault) source, we use eq. A-1 of Kanamori and Stewart (1976), and replace (14) by

$$\hat{V}_\phi(\mathbf{r}, \omega) = M_0 (p_L P_L^{(1)} + i q_L Q_L^{(1)}) \quad (16)$$

where p_L and q_L are determined by the fault parameters.

3. Analysis

From the observed seismograms of Rayleigh or Love waves, we obtain $\hat{V}_r(\mathbf{r}, \omega)$ for Rayleigh waves or $\hat{V}_\phi(\mathbf{r}, \omega)$ for Love waves. Then, the moment tensor or the fault parameters can be determined by inverting (6) or (12) for Rayleigh waves, and (14) or (16) for Love waves.

We shall now describe the analysis method for Rayleigh waves obtained from the IDA records. However, essentially the same method would apply to other kinds of records.

3.1. Period

Equation 6 or 12 can be solved at any period $T = 2\pi/\omega$. In our experience, it is relatively easy to obtain Rayleigh wave data up to 350 s from the IDA records of large earthquakes. Since the sampling interval of the IDA data is 20 s (i.e. the Nyquist period is 40 s), it is probably not safe to use periods shorter than about 100 s. Furthermore, propagation of Rayleigh waves with periods less than 100 s is strongly affected by the lateral heterogeneity of the Earth's structure. We therefore use Rayleigh waves with periods between 180 and 350 s.

There is one difficulty in using very long-period waves for the inversion of source parameters of shallow-focus earthquakes. The excitation function

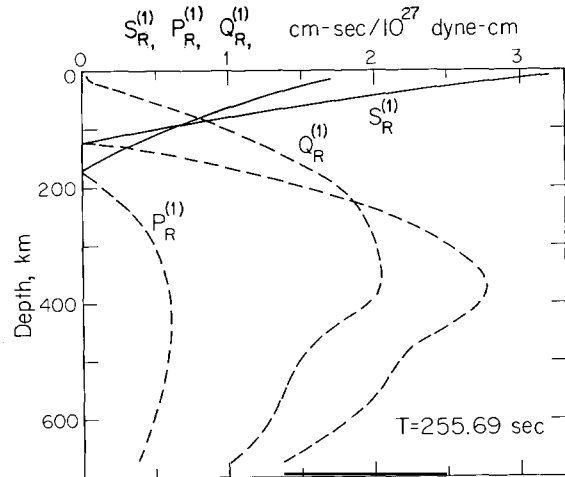


Fig. 2. The excitation functions $S_R^{(1)}$, $Q_R^{(1)}$ and $P_R^{(1)}$ at the period of 255.69 s. The dotted curves indicate negative values.

$Q_R^{(1)}$ (or $Q_L^{(1)}$ for Love waves) is derived from the radial factor of the stress function of normal modes (e.g. Kanamori and Stewart, 1976), which vanishes at the Earth's surface. For very long-period waves, most shallow events have essentially a surface focus, and $Q_R^{(1)}$ becomes very small. Since $Q_R^{(1)}$ is the coefficient of M_{xz} and M_{yz} in (5), the small values of $Q_R^{(1)}$ make the determination of M_{xz} and M_{yz} very unstable. In the limit of zero depth, M_{xz} and M_{yz} become indeterminate. Further discussion on this point will be made later.

The excitation functions $P_R^{(1)}$, $S_R^{(1)}$, $Q_R^{(1)}$ for fundamental-mode Rayleigh waves at $T=256$ s are shown in Fig. 2. These are computed for the Earth model 5.08 M (Press, 1970; Kanamori, 1970). The Rayleigh and Love wave excitation functions for various periods and depths are given in the Appendix.

3.2. Finiteness

In the preceding discussion, a step-function point source was assumed. If the Rayleigh waves with a period of 150–350 s are used, the wavelength is about 1000 km, so this assumption is reasonably good for most events smaller than $M_S = 7$. However, it is not valid for very large events, and corrections are necessary for the amplitude and, in particular, the phase spectrum. A large earthquake may be modeled by a propagating dislocation. Strictly speaking, a finite source cannot be represented by a first-order moment tensor and higher-order moment tensors are required to formulate the excitation problem. This difficulty may be circumvented, at least partially, by using a source finiteness function introduced by Ben-Menahem (1961). If the time history of the dislocation at a point on the fault (local dislocation function) is given by $s(t)$ with its Fourier transform $\hat{s}(\omega)$, then uniform propagating source can be approximated by a point source whose frequency spectrum is

$$\hat{s}(\omega)\hat{f}(\omega) \quad (17)$$

where $\hat{f}(\omega)$ represents the effect of the source finiteness. For a unilateral propagating source with a fault length L

$$\hat{f}(\omega) = \frac{\sin X}{X} \exp(-iX) \quad (18)$$

where

$$X = \frac{\omega L}{2V_0} \left(1 - \frac{V_0}{C} \cos \Theta \right) \quad (19)$$

Here, V_0 is the rupture velocity, C the phase velocity, and Θ the azimuth of the station measured from the rupture direction. For bilateral faulting and two-dimensional rupture propagation (18) needs to be modified.

Thus, for a finite source with a dislocation time history $s(t)$, \hat{V}_r in (5), which is for a step-function point source, should be replaced by $\hat{V}_r i\omega\hat{s}(\omega)\hat{f}(\omega)$, where $(i\omega)^{-1}$ represents the step-function point source. Then two methods can be used to solve the modified eq. 5. First, if the azimuthal variation of $\hat{f}(\omega)$ can be ignored (it is probably small for a bilateral or circular faulting) then we can absorb the unknown term $\hat{s}(\omega)\hat{f}(\omega)$ in the source moment tensor by moving the $i\omega\hat{s}(\omega)\hat{f}(\omega)$ term from the left-hand to the right-hand side of (5). We then define a complex moment tensor M'_{xy} , etc. by $M'_{xy} = M_{xy} (i\omega\hat{s}(\omega)\hat{f}(\omega))^{-1}$, etc. In this case, the inversion of (7) should be made for 10 unknowns (the real part and the imaginary part of M'_{xy} , etc.) instead of five. This procedure is similar to that used by Dziewonski and Gilbert (1974). In the second method, we compute $\hat{s}(\omega)\hat{f}(\omega)$ for a rupture model to correct \hat{V}_r for the source finiteness.

If a large number of stations are available, the first method is more general. However, if the azimuthal variation of the source finiteness is very large, this method cannot be used. Since a relatively small number of stations are used in the present study, we use the second method to correct for the source finiteness.

3.3. Phase velocity, Q , group velocity and instrument response

To obtain \hat{V}_r from the observed spectrum \hat{U}_r , the values of the phase velocity C , Q , the group velocity U and the instrument response are required. For C we used the average observed normal-mode periods compiled by Gilbert and

TABLE I
Normal-mode data (Gilbert and Dziewonski, 1975)

n	${}_0S_n$ (s)	${}_0T_n$ (s)
16	406.78	429.18
17	389.32	410.24
18	374.02	390.94
19	360.23	374.76
20	347.69	359.59
21	336.00	346.07
22	325.30	333.15
23	315.44	321.21
24	306.29	310.36
25	297.72	300.19
26	289.69	290.26
27	282.34	281.35
28	275.20	272.91
29	268.45	264.93
30	262.15	257.29
31	256.07	250.29
32	250.34	244.26
33	244.95	237.37
34	239.70	231.29
35	234.69	224.93
36	229.86	220.70
37	225.22	213.89
38	220.75	209.83
39	216.48	204.27
40	212.41	199.96
41	208.39	195.88
42	204.58	191.26
43	200.93	187.40
44	197.40	183.78

Dziewonski (1975), after converting them into phase velocities. The values are shown in Table I. Since the regional variation of phase velocities is relatively small at the period of about 250 s, the same phase velocity is used for all the paths.

TABLE II
Group velocity and Q

T (s)	Rayleigh wave velocity U (km s ⁻¹)	Q	Love wave velocity U (km s ⁻¹)	Q
175	3.62	147	4.39	122
200	3.59	171	4.39	111
225	3.58	179	4.39	113
250	3.59	189	4.40	112
275	3.64	185	4.41	116
300	3.71	183	4.41	110
325	3.78	182	4.41	108

However, it would be desirable to incorporate the regional variation when more data become available.

For the group velocity and Q , which are necessary to compute the attenuation term $\exp(\omega a \theta' / 2QU)$, we used the values taken from Kanamori (1970), which are given in Table II. For the instrument response we used the transfer functions and the constants provided by the IDA project team at the Institute of Geophysics and Planetary Physics, University of California, San Diego.

3.4. Group velocity window

The Rayleigh wave trains used for the analysis were filtered through the following group velocity windows:

$$R_1 \quad 3.10\text{--}4.90 \text{ km s}^{-1}$$

$$R_2 \quad 3.30\text{--}3.90 \text{ km s}^{-1}$$

$$R_n, n \geq 3 \quad 3.35\text{--}3.80 \text{ km s}^{-1}$$

Each filtered trace was tapered by cosine functions at the beginning and the end. The length of record that was tapered at each end was about 15% of the total length. The three group velocity windows are for the standard case; they were occasionally varied slightly according to the distance of the stations and the quality of the record.

3.5. Constraints

When the source is very shallow, $Q_R^{(1)}$ is very small so that the determination of M_{xz} and M_{yz} becomes very difficult. In our experience, when the depth is larger than 30 km, M_{xz} and M_{yz} can be determined well. However, when the depth is shallower than 30 km, they become practically indeterminate. In other words, we can determine only three moment tensor elements out of five. Since at least four parameters are necessary to determine a fault model, the fault mechanism becomes indeterminate. We use two methods to overcome the difficulty. In the first, we constrain one or more fault parameters (e.g. dip angle, fault strike) on the basis of other data, such as the P-wave first motions, or of geological considerations (the geome-

try of the surface break, strike of the trench, etc.), and use (12) to determine other parameters. Although the solution is not entirely objective, this method often yields reasonable solutions.

In the second method, we constrain M_{xz} and M_{yz} to be equal to zero, and solve (7) for the three unknowns M_{xx} , M_{yy} , and M_{xy} . The constraints $M_{xz} = M_{yz} = 0$ are equivalent to constraining the fault mechanism to be either a pure-strike slip on a vertical fault (vertical strike slip) or a pure-dip slip on a fault dipping 45° (45° -dip slip) (eq. 1 of Mendiguren, 1977). In effect we look for the best solution from a subset of fault models that consists of vertical-strike slip faults or 45° -dip slip faults. Although this solution may appear too restrictive, it actually provides a very useful first approximation. If the actual mechanism is close to either one of these mechanisms, the fault type, the strike azimuth, the seismic moment and the sense of the motion are very well determined. However, if the mechanism has a large oblique slip component, the solution is inevitably subject to considerable error.

The advantage of the second method is that a good first approximation can usually be obtained objectively without an initial guess. Once the first approximation is obtained, further refinement could be made on the basis of other geophysical or geological considerations. For example, if a 45° thrust mechanism is obtained for an event along a subduction zone where the dip angle of other events is consistently about 20° , as is usually the case, then we may constrain one of the nodal planes to have a dip angle of 20° and the same strike azimuth as the first approximation, and repeat the inversion by using (12).

Thus, the difficulties that arise from the inherent indeterminacy of M_{xz} and M_{yz} for very shallow events can usually be overcome by introducing additional constraints on the basis of other geophysical and geological data.

For deeper events, all of the five moment tensor elements can be determined well. However, at depths where $P_R^{(1)}$ or $S_R^{(1)}$ vanishes (e.g. at 170 km and 120 km for the period of 255.69 s; Fig. 2), a similar difficulty arises. This difficulty can be overcome, however, by using different periods or overtones, or both.

3.6. Depth

Since we use very long-period waves over a relatively narrow period range (150–350 s at most), the depth of the events cannot be determined very well. Usually a point source or a distributed source is assumed at a depth determined by other methods.

Since we are primarily concerned with large events with a linear dimension of 30 km or more, a distributed source is probably more adequate than a point source. We computed excitation functions for several distributed sources that extend from the surface to a depth d_M . We assumed that the dislocation is uniform on the fault plane. In this case the excitation function $P_R^{(1)}$ for a distributed source extending from 0 to d_M is given by

$$P_{R,d_M}^{(1)} = \frac{\int_0^{d_M} \mu(h) P_R^{(1)}(h) dh}{\int_0^{d_M} \mu(h) dh} \quad (20)$$

where $\mu(h)$ and $P_R^{(1)}(h)$ are the rigidity and the excitation function as functions of depth. The excitation functions for various d_M are computed and tabulated in the Appendix.

3.7. Other corrections

Since the values of phase velocities and Q for a gross Earth model are used in the present method, the regional variation in these parameters can introduce errors in the source phase and the amplitude. Although the errors in the amplitude would not cause very serious error in the source parameters, those in the phase can be very serious. At the period of 250 s, the 0.05% variation of the phase velocity, quoted as error by Gilbert and Dziewon-ski (1975), could introduce errors of 0.025, 0.074, 0.12, 0.17 and 0.22 rad for travel distances of 90, 270, 450, 630 and 810°, typical distances for R_1 , R_2 , R_3 , R_4 and R_5 respectively. Errors of this magnitude would not cause serious errors in the source parameters (Patton and Aki, 1979). However, the 0.05% variation is a gross average, and a much larger variation (e.g. 0.2%) is possible for very anomalous paths. In such a case a very large

error in the source phase is caused, particularly for multiple surface waves with a large order number (e.g. R_4 and R_5).

The source finiteness and the finite source rise time cause a finite phase shift. Uncertainties in these parameters would cause errors in the source phase. The correction for the source finiteness can be made by using the method described earlier, if the details of the rupture mode are known. If they are unknown, we assume that the overall source finiteness effect is given by

$$\frac{\sin(\pi\tau/T)}{(\pi\tau/T)} \exp(-i\pi\tau/T) \quad (21)$$

where T is the period of the wave used, and τ is the time for the overall source process to be completed. The finiteness term is assumed to be nondirectional. This is not true for a unilateral or bilateral rupture, but is a reasonably good approximation for a fault length of up to 100 km. The source process time τ may be approximately equal to the fault length divided by the rupture velocity. Since the logarithm of the fault length is approximately proportional to the earthquake magnitude, we used an empirical relation shown by Table III to estimate τ . A recent study by Furumoto (1979) on the initial phase of Rayleigh waves excited by great earthquakes confirms that the source process times given in Table III are appropriate. Additional errors in the source phase arise from errors in the earthquake origin time and in the timing of the record, although these are relatively rare. An earthquake is sometimes preceded by a small ‘precursory’ event, and the origin time refers to this event rather than the main event. The time difference between the precursory

TABLE III

Empirical relations between M_w and the source process time

M_w	L (km)	τ (s)
9.5	1000	330
9.0	560	190
8.5	320	110
8.0	180	59
7.5	100	33
7.0	56	19
6.5	32	11

event and the main event is in effect the ‘error’ in the origin time. The effect of these errors on the estimation of source parameters is discussed in detail by Patton and Aki (1979).

If Δt is the sum of timing errors resulting from the regional variation of phase velocities, incomplete knowledge of the source finiteness, the origin time and the clock errors, the error in the source phase at period T is $2\pi\Delta t/T$. Although there is no direct way to estimate this error, it is often possible to estimate it from the phases of multiple surface waves recorded at the same station, if the errors do not depend on the azimuth. As shown by (5), for a step-function point source the spectrum \hat{V}_r of the R_{2n} phase should be the complex conjugate of that of the R_{2n+1} phase at the same station. Therefore, if the phase of R_{2n} is ϕ_0 then the phase of R_{2n+1} must be $-\phi_0$ for a point source. For a nondirectional finite source with a possible error Δt , the phase of R_{2n} is $\phi'_1 = \phi_0 - (X + 2\pi\Delta t/T)$ and that of R_{2n+1} is $\phi'_2 = -\phi_0 - (X + 2\pi\Delta t/T)$. Adding these two, we have

$$(\phi'_1 + \phi'_2)/2 = -(X + 2\pi\Delta t/T)$$

Thus if we assume that the errors do not depend on the azimuth, we can estimate the unknown phase correction $(X + 2\pi\Delta t/T)$ by taking the average of ϕ'_1 and ϕ'_2 . To do this, we need both R_{2n} and R_{2n+1} (e.g. R_1 and R_2). When the fault length is much larger than 100 km, the azimuthal variation of the finiteness effect becomes significant so that this method would introduce a bias in the source phase, unless the directional finiteness effect is removed by the method described earlier.

Since the situation encountered varies considerably from event to event, further details are discussed for actual examples in the following sections.

4. Examples

4.1. Miyagi-Oki, Japan, earthquake June 12, 1978

The source parameters of this earthquake given by the National Earthquake Information Service (NEIS) are:

Origin time: 8 h 14 min 26.4 s
 Latitude: 38.190°N; longitude: 142.028°E
 Depth: 44 km
 $M_s = 7.7$

Seno et al. (1980) made a detailed analysis of this event, and showed that it consisted of two distinct events 11 s apart. Since the period used in our analysis is much longer than 11 s, we treat this earthquake as a single event.

The aftershock area of this earthquake was determined very well (Tohoku University, 1979) and suggests that the faulting extends to a depth of about 50 km. We therefore use a depth of 43 km for the point source in our inversion. If the depth is larger than 30 km, all of the five moment tensor elements can be determined. For comparison, we first constrained M_{xz} and M_{yz} to be equal to zero, and inverted the data at $T = 256$ s. The stations and phases used are shown in Fig. 3, and the results are shown in Table IV and Fig. 4a. This solution essentially represents one double couple (the moment of the minor double couple is 2% of the major double couple). We then removed the constraints $M_{xz} = M_{yz} = 0$, and obtained the results shown in Table IV and Fig. 4b. The mechanism shown in Fig. 4b is in good agreement with the result obtained by Seno et al. (1980). Since the

dimension of the combined rupture zone of this event is about 70 km (Seno et al., 1980), the effect of the source finiteness is probably very small. For comparison, we used a source process time τ of 30 s for this earthquake. In effect, a constant phase of 0.37 rad (i.e. $\pi\tau/T$) is added to all the data. As can be seen in Table IV, inclusion of this correction considerably reduces the standard errors of the estimates of the moment tensor elements, suggesting that the correction is appropriate. As shown in Fig. 4c, the geometry of the mechanism remains essentially the same. The overall fit of the phase and the amplitude of this solution with the data is shown in Fig. 3.

Comparing Figs. 4a and c, we find that the constrained solution gives approximately the correct strike azimuth. The seismic moment is smaller for this solution because the excitation of surface waves by a dip-slip source is proportional to $M_0 \sin 2\delta$; for a given observed amplitude the moment is proportional to $1/\sin 2\delta$.

To check the overall consistency of this solution, synthetic seismograms are computed by the method of Kanamori and Cipar (1974) and compared with the observed seismograms in Fig. 5.

Only fundamental modes are included in the synthesis, and a Gaussian bandpass filter with a passband from 150 to 1500 s is applied to both the

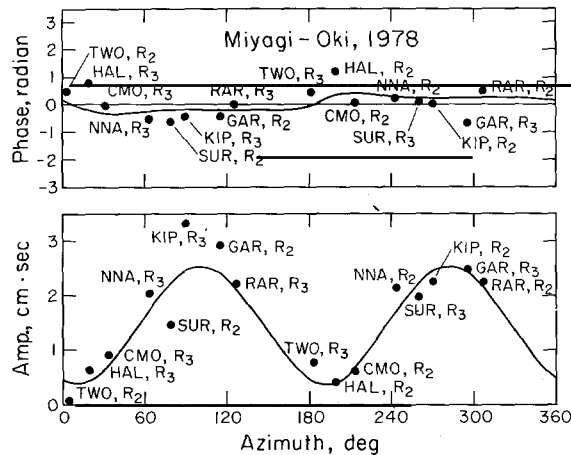


Fig. 3. Phase and amplitude spectra of the Miyagi-Oki earthquake. Phase spectra have been corrected for the source finiteness by using $\tau = 30$ s. The full curves were computed for model 3 in Table IV. The time for the KIP data is corrected by using the arrival time of the P-wave.

TABLE IV

Miyagi-Oki, Japan, earthquake, 1978 ($d = 43$ km): moment tensor (units of 10^{20} Nm = 10^{27} dyne·cm)

(1) Constrained solution ($M_{xz} = M_{yz} = 0$)

$$\begin{aligned} M_{xy} &= -0.319 \pm 0.274 \\ M_{yy} - M_{xx} &= -1.11 \pm 0.48 \\ M_{yy} + M_{xx} &= -1.23 \pm 0.22 \end{aligned}$$

(2) Unconstrained

$$\begin{aligned} M_{xy} &= -0.319 \pm 0.268 \\ M_{yy} - M_{xx} &= -1.11 \pm 0.47 \\ M_{yy} + M_{xx} &= -1.23 \pm 0.21 \\ M_{yz} &= -1.41 \pm 0.76 \\ M_{xz} &= -0.223 \pm 0.892 \end{aligned}$$

(3) Unconstrained (phase corrected, $\tau = 30$ s)

$$\begin{aligned} M_{xy} &= -0.340 \pm 0.168 \\ M_{yy} - M_{xx} &= -1.53 \pm 0.30 \\ M_{yy} + M_{xx} &= -1.39 \pm 0.13 \\ M_{yz} &= -1.49 \pm 0.48 \\ M_{xz} &= -0.133 \pm 0.560 \end{aligned}$$

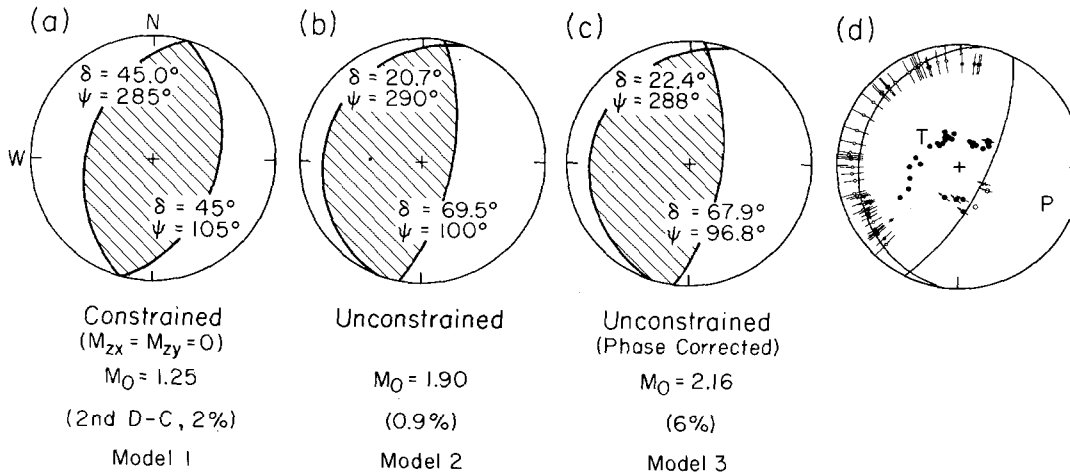


Fig. 4. The mechanisms of the major double couples obtained by moment tensor inversion (a, b, c) and (d) the solution obtained by Seno et al. (1980). Equal area projection of the lower focal sphere is shown. Hatched areas and full circles represent compressional quadrants.

synthetic and the observed records. As shown by Fig. 5, the agreement is good in both the amplitude and the phase. Although good agreement of the waveform does not necessarily mean that the mechanism is correct, this comparison is useful for checking the overall quality of the data and the solution.

4.2. Colombia-Ecuador earthquake, December 12, 1979

The source parameters given by NEIS are:

Origin time: 7 h 59 min 3.30 s
 Latitude: 1.598°N; longitude: 79.358°W
 Depth: 24 km
 $M_s = 7.7$

This was a large earthquake with a very large rupture length; therefore the point source approximation is clearly inadequate. To compare the effect of the various assumptions for the source finiteness described earlier, we inverted the data for four cases: (1) constrained ($M_{xz} = M_{yz} = 0$) solution without correction for the source finite-

ness; (2) constrained ($M_{xz} = M_{yz} = 0$) solution with a uniform source process time of 60 s (Table III); (3) unconstrained solution with a uniform source process time of 60 s; (4) unconstrained solution with source phase and amplitude corrections derived from the inferred rupture model. The depth of the point source used is 33 km. The source process time τ of 60 s corresponds to $M_w = 8$ (Table III). The corresponding source models are shown by Fig. 6 and Table V.

This analysis was made to investigate the applicability of the method to a real-time tsunami warning system. Since the size of the earthquake is not known in the beginning, the first inversion was made without any corrections for the source finiteness. In this case, the fit is expected to be poor and the inversion would be very unstable unless M_{xz} and M_{yz} are constrained. As model 1 in Table V and Fig. 6(a) shows, a 45° thrust mechanism with a seismic moment of 1.01×10^{28} dyne·cm ($M_w = 7.9$) was obtained. Although the finiteness parameters are unknown at this stage, the value of M_w suggests a source process time of about 60 s (Table III). The second and third inversions were then made using this constant source process time with

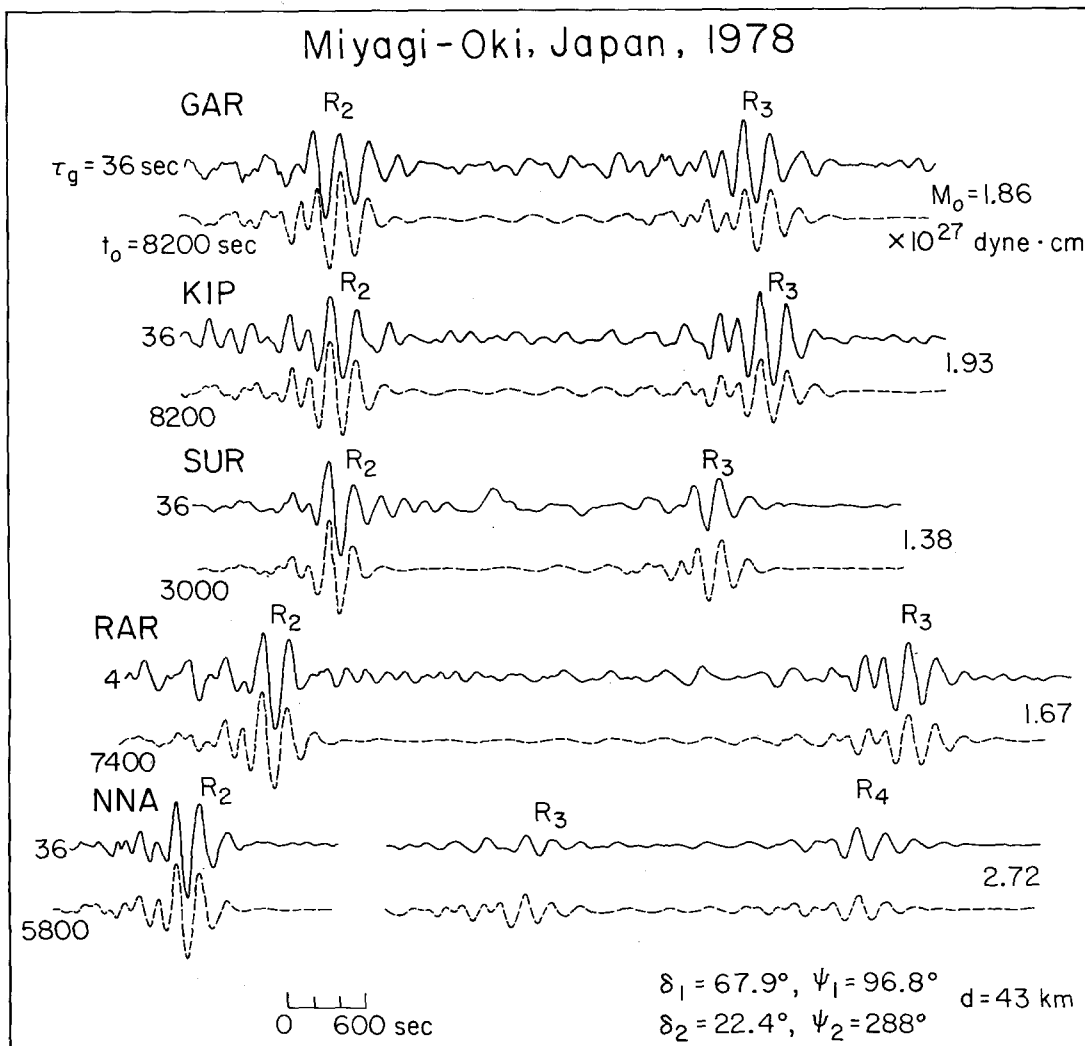


Fig. 5. Comparison of the observed seismograms (full curves) with the synthetic (dotted) curves computed for model 3 in Table IV. τ_0 is the starting time of the synthetic measured from the origin time; τ_g is the group delay time for the observed seismograms relative to the synthetics. M_0 is the seismic moment used for the synthetics.

and without the constraints $M_{xz} = M_{yz} = 0$, respectively. As model 2 in Table V and Fig. 6(b) shows, the mechanism is essentially identical to that of model 1. However, the standard errors and root mean square errors are substantially reduced. As model 3 in Table V shows, the standard errors for the unconstrained solution are small. The mechanism obtained is a low-angle thrust fault dipping east (or a high-angle fault dipping west) and is consistent with the geometry of subduction

of the Nazca plate beneath South America (Fig. 6(c)). In fact, this solution is consistent with the first-motion data obtained from the WWSSN stations (Fig. 7), and is essentially identical to model 4 in Table V and Fig. 6(d), which is obtained by a more detailed analysis to be described below. It is encouraging that model 3, which can be obtained without any detailed knowledge of the rupture length, direction and mode, gives a very good solution. Since the analysis up to model 3 can be

TABLE V

Colombia-Ecuador Earthquake, 1979: moment tensor (units of 10^{20} Nm = 10^{27} dyne · cm) ($d=33$ km). δ_i is the dip angle and ψ_i the dip direction

Model	1	2	3	4
τ (s)	0	60	60	Variable
M_{xy}	-2.26 ± 2.98	-3.62 ± 2.19	-3.62 ± 2.00	-4.37 ± 1.99
$M_{yy} - M_{xx}$	-12.7 ± 8.6	-15.2 ± 6.3	-15.2 ± 5.8	-15.7 ± 5.7
$M_{yy} + M_{xx}$	-6.80 ± 2.44	-11.4 ± 1.8	-11.4 ± 1.6	-15.1 ± 1.6
M_{yz}	0	0	28.2 ± 10.4	24.4 ± 10.4
M_{xz}	0	0	-1.01 ± 10.29	-2.42 ± 10.23
Major double couple				
M_0	10.1	14.1	31.9	29.2
δ_1 (°)	45	45	16	20
ψ_1 (°)	100	103	121	121
δ_2 (°)	45	45	78	74
ψ_2 (°)	280	283	269	268
Minor				
double couple (%)	33	19	5.6	0.2
Root				
mean square error	10.7	7.90	7.21	7.17

completed almost instantly after the seismograms have been retrieved, this method holds good promise for real-time tsunami warning applications.

We made a further analysis of this event to determine the rupture mode. For a very large event whose rupture length is larger than 300 km, the rupture mode can be determined by using the directivity function introduced by Ben-Menahem (1961). However, this earthquake is not large enough to yield the spectral holes of the directivity function at periods where the signal-to-noise ratio

is large. We therefore used a different method. First we computed synthetic seismograms by using a step-function point source with the fault geometry given by model 3. The synthetic and observed seismograms were bandpass-filtered with a pass-

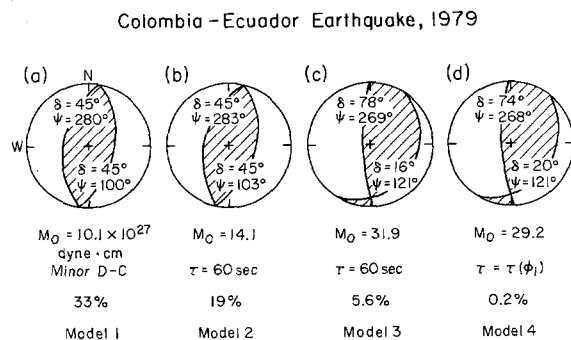


Fig. 6. Mechanisms of the major double couple determined by the moment tensor inversion. Hatched areas represent the compressional quadrant. Stereographic projection of the lower hemisphere is shown.

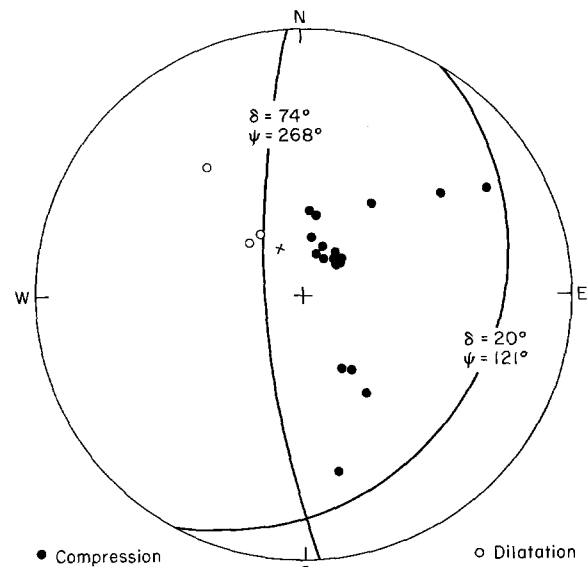


Fig. 7. Comparison of the first-motion data (full circle: compression; open circle: dilatation) and model 4 shown in Fig. 6.

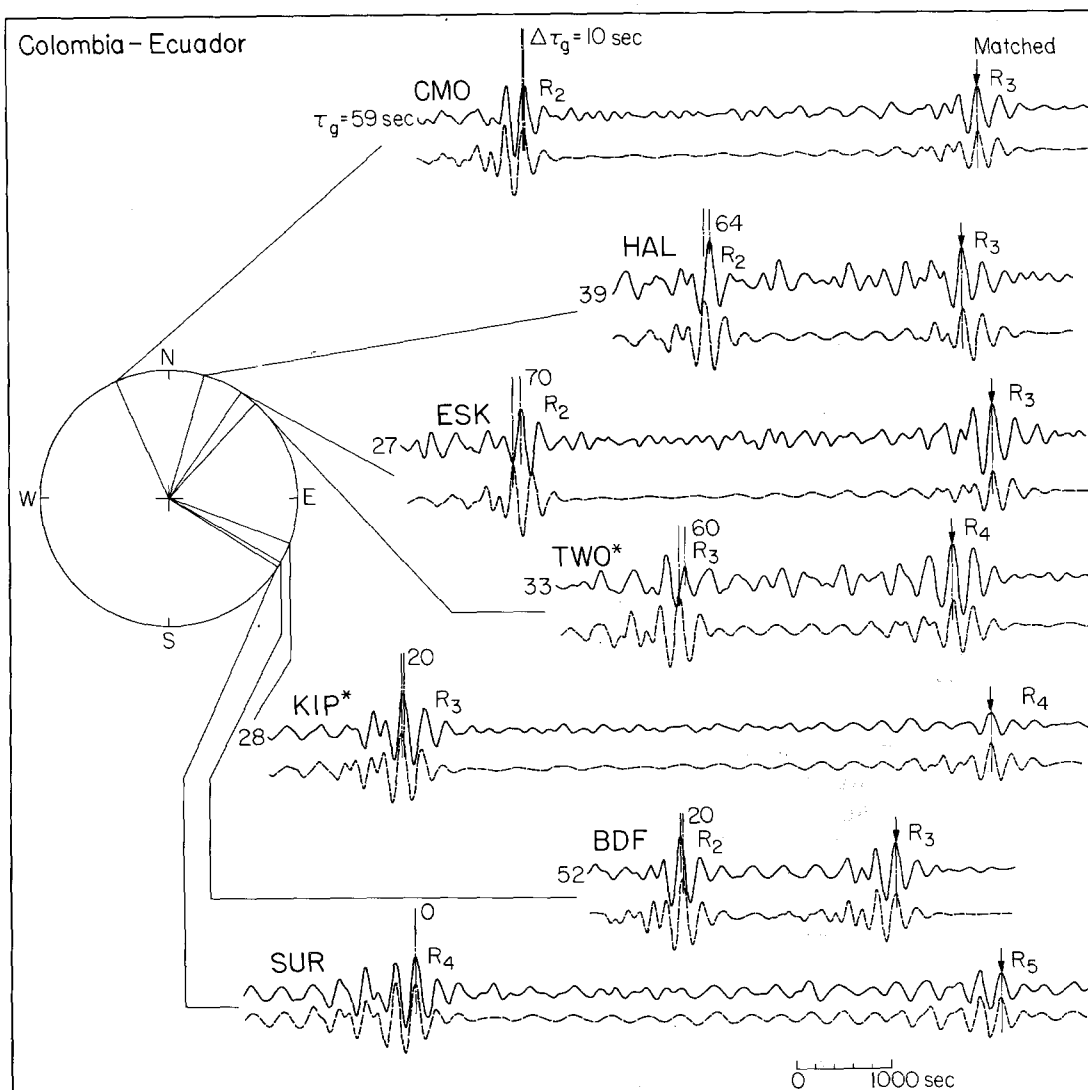


Fig. 8. Comparison of the observed seismograms (full curves) with the synthetics (dotted curves) computed for model 3 shown in Fig. 6. τ_g is the group delay of the observed seismograms relative to the synthetics. Observed and synthetic seismograms are aligned at the point indicated by a downward arrow. $\Delta\tau_g$ is the group delay time of the Rayleigh waves propagated in the south-west azimuth with respect to those in the north-east azimuth. The largest delay for ESK R_2 propagated in S 34° W. The asterisk indicates the station plotted in the azimuth opposite to the station azimuth.

band from 150 to 1500 s and are compared in Fig. 8. As shown, the observed Rayleigh waves are always delayed with respect to the corresponding synthetics. The delays are larger at stations in the southwest azimuth from the source and smaller in the northeast azimuth. In other directions the delays are, on the average, intermediate. This ob-

servations can be interpreted in terms of the source group delay caused by a unilateral rupture propagation in the north-east direction. Using (19) we can express the source group delay by

$$\tau_g = \frac{dX}{d\omega} = \frac{L}{2V_0} \left(1 - \frac{V_0}{U} \cos \Theta \right) \quad (22)$$

For a station with azimuth Φ , $\Theta = \Phi - \Phi_0$ where Φ_0 is the rupture direction. Therefore, from (22)

$$\Delta\tau_g \equiv \tau_g(\Phi + \pi) - \tau_g(\Phi) = \frac{L}{U} \cos(\Phi - \Phi_0) \quad (23)$$

and

$$\bar{\tau}_g = \frac{1}{2} [\tau_g(\Phi + \pi) + \tau_g(\Phi)] = \frac{L}{2V_0}. \quad (24)$$

Figure 9 shows $\Delta\tau_g$ and $\bar{\tau}_g$ for the stations of Fig. 8. The group delay times are measured for the wave train with the period of about 225 s (Airy phase). From Fig. 9(b), Φ_0 and L/U are estimated to be 40° and 65 s respectively. Since $U = 3.56 \text{ km s}^{-1}$, the estimate of L/U gives $L = 230 \text{ km}$. From Fig. 9(a), $L/2V_0$ is estimated to be 57 s, from which the rupture velocity V_0 is estimated to be 2 km s^{-1} . We have assumed that the group velocity does not depend on the path. The systematic pattern shown by Fig. 9 suggests that this assumption is reasonable in the present case. We can now use these parameters to correct for the source finiteness by using (18) and (19). Model 4 of Table V and Fig. 6(d) is obtained in this manner. The overall fit of the amplitude and phase is shown in Fig. 10.

Comparison of the four models shown in Fig. 6

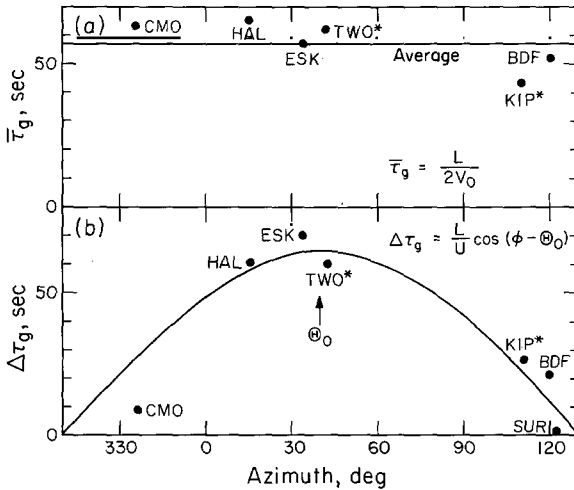


Fig. 9. Variation of group delay times as a function of azimuth (a). The group delay times are measured from Fig. 8, and corrected for the ellipticity of the Earth. The full curve in (b) is a half-cycle of cosine wave fitted to the data. The asterisk indicates the station plotted in the azimuth opposite to the station azimuth.

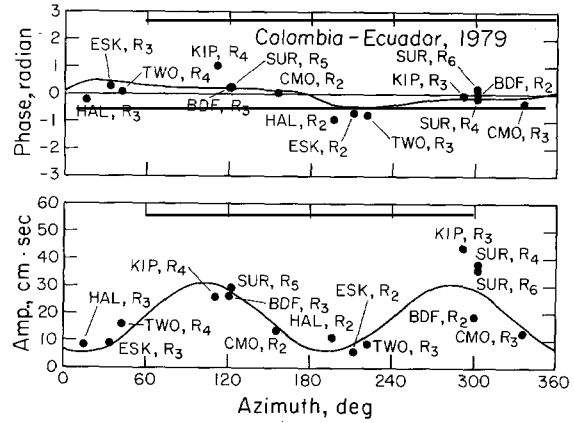


Fig. 10. Phase and amplitude spectra of the Colombia-Ecuador earthquake. Phase spectra are corrected for the finiteness with $L = 230 \text{ km}$, $V_0 = 2 \text{ km s}^{-1}$, $\Theta_0 = 40^\circ$. The full curves are computed for model 4 in Table V. The time for the SUR data is calibrated by using the arrival time of the P-wave.

demonstrates that the constrained solution gives approximately correct fault geometry and fault strike. Hence, if the source is very shallow and the unconstrained inversion is not possible, we can use the constrained solution as a useful first approximation.

4.3. Monte Negro, Yugoslavia, earthquake, April 15, 1979

The source parameters given by NEIS are:

Origin time: 6 h 19 min 44.1 s
 Latitude: 42.096°N ; longitude: 19.209°E
 Depth: 10 km
 $M_s = 6.9$

The depth of this event is somewhat uncertain. To obtain the first approximation we first constrained M_{xz} and M_{yz} to be 0, and inverted the data shown in Fig. 11. We assumed a distributed source extending to a depth of 24.5 km and used $\tau = 10 \text{ s}$. The results are shown in Table VI and Fig. 12(a). The first-motion data for this event (Boore et al., 1981) cannot constrain the mechanism unambiguously, but they determine one of the nodal planes. The plane dips 75° in the direction of $\text{S}31^\circ\text{W}$ (or a strike of 301°); this is in close

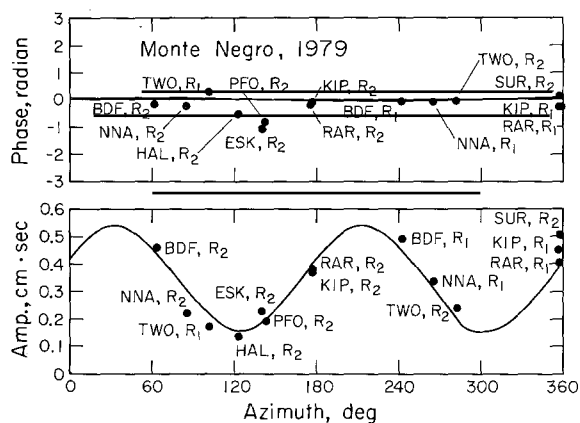


Fig. 11. Phase and amplitude spectra of the Monte Negro earthquake. Phase spectra are corrected for the source finiteness with $\tau=10$ s. The full curves are computed for model 2 in Table VI.

agreement with the strike of the nodal planes determined by the moment tensor inversion.

If we assume that the sources for the body waves and long-period surface waves are the same, we can invert the surface wave data by constraining the plane determined by the first-motion data. The results of this inversion are shown in Table VI

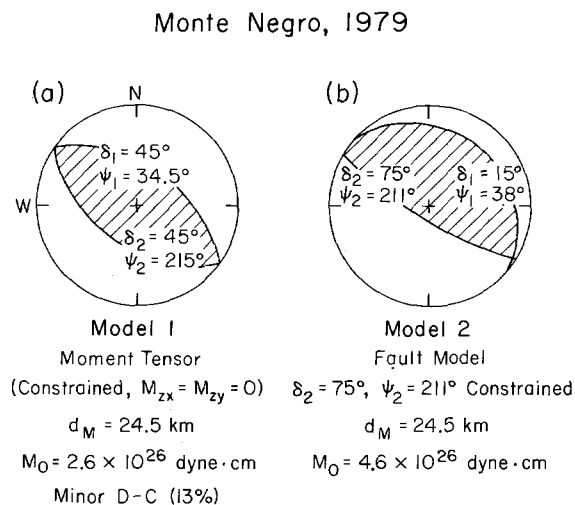


Fig. 12. The mechanism diagrams of the Monte Negro earthquake. Model 1 is the constrained ($M_{xz} = M_{yz} = 0$) moment tensor solution and model 2 is the fault plane solution with one nodal plane constrained by the first-motion data. Stereographic projection of the lower focal sphere is shown. Hatched areas represent compressional quadrant.

TABLE VI

Monte Negro, Yugoslavia, earthquake, 1979: moment tensor (units of 10^{20} Nm = 10^{27} dyne·cm) δ_i is the dip angle and ψ_i is the dip direction

(1) Constrained solution ($M_{xz} = M_{yz} = 0$)

$$d_M = 24.5 \text{ km}, \tau = 10 \text{ s}$$

$$M_{xy} = 0.138 \pm 0.022$$

$$M_{yy} - M_{xx} = 0.106 \pm 0.028$$

$$M_{yy} + M_{xx} = -0.228 \pm 0.013$$

Equivalent double couple

Major double couple

$$M_0 = 2.6$$

$$\delta_1 = 45.0^\circ, \psi_1 = 34.5^\circ$$

$$\delta_2 = 45.0^\circ, \psi_2 = 215^\circ$$

Minor double couple (13%)

(2) Fault model

$$d_M = 24.5 \text{ km}, \tau = 10 \text{ s}$$

$$M_0 = (4.6 \pm 0.3)$$

$$\delta_1 = 15^\circ, \psi_1 = 38^\circ$$

$$\delta_2 = 75^\circ, \psi_2 = 211^\circ \text{ (constrained)}$$

and Fig. 12(b). The mechanism is essentially a pure dip-slip fault. Figure 13 compares the synthetics computed for the mechanism shown in Fig. 13(b) and the observed seismograms.

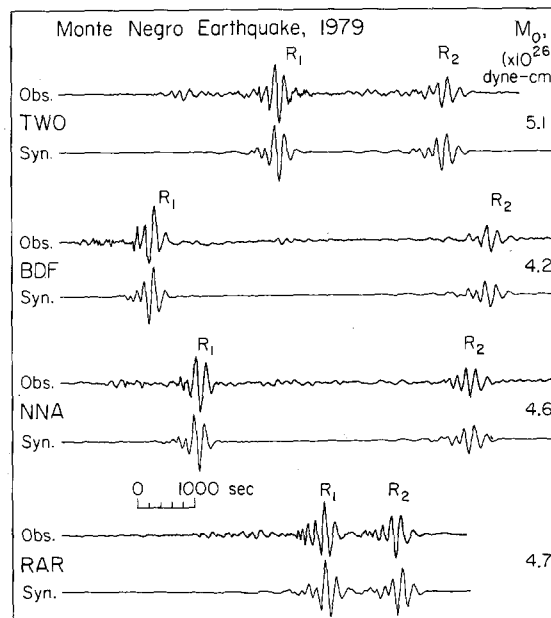


Fig. 13. Comparison of the observed (upper lines) and synthetic seismograms (lower lines) computed for model 2 shown in Table VI.

4.4. Izu-Oshima, Japan, earthquake, January 14, 1978

The source parameters of this earthquake given by NEIS are:

Origin time: 3 h 24 min 39.0 s
 Latitude: 34.809°N; longitude: 139.259°E
 Depth: 14 km
 $M_s = 6.6$

Shimazaki and Somerville (1979) determined the source parameters of this earthquake by using far-field SH waves, near-field strong-motion records, surface waves and static data. Since this event is relatively small, the signal-to-noise ratio of long-period Rayleigh waves recorded at IDA stations is relatively low. Furthermore, the vertical extent of the fault is about 10 km so that M_{xz} and M_{yz} are almost indeterminate. Hence, the inversion was attempted only for the constrained solution. A depth of 16 km is used for the point source. The results are presented in Figs. 14 and 15 and Table VII. As shown by Fig. 14, the constrained solution gives a 90° strike slip solution, which is in close agreement with the result obtained by Shimazaki and Somerville (1979). The relatively large minor double couple obtained for this event may be due to the complex fault geometry as delineated by the

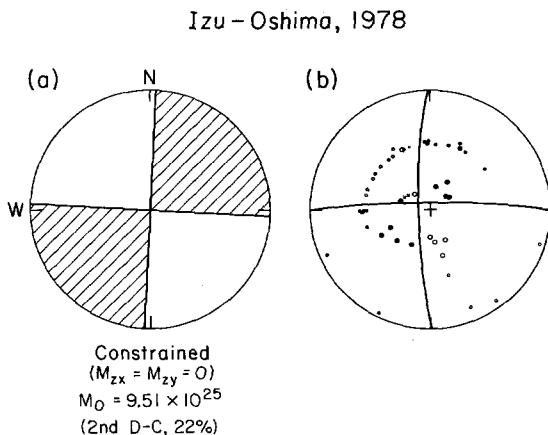


Fig. 14. The mechanism diagram of the Izu-Oshima earthquake. The major double couple of the moment tensor (a) and the mechanism determined by Shimazaki and Somerville (1979) are shown. Hatched areas represent the compressional quadrant.

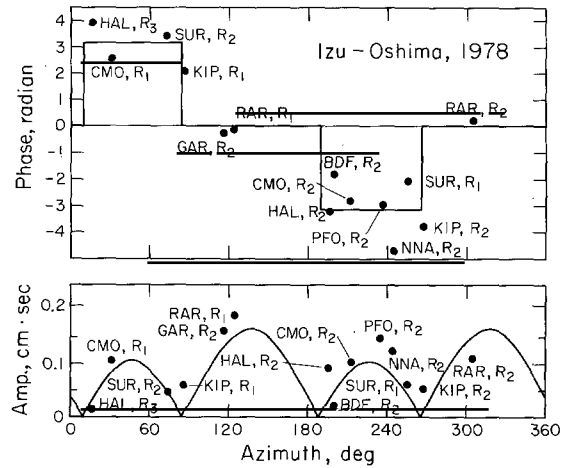


Fig. 15. Phase and amplitude spectra of the Izu-Oshima earthquake. The full curves are computed for the model shown in Table VII and Fig. 14.

foreshock and the aftershocks. However, in view of the fairly large standard errors, the minor double couple should not be given much significance.

5. Conclusion

As we have demonstrated in the previous section, the method developed here can be used for rapid retrieval of earthquake source parameters. Although the source moment tensor cannot be determined completely for very shallow events, a good first approximation can usually be obtained by constraining two of the five moment tensor elements. Further improvement of the solution can be made by incorporating other geological and geophysical data, such as the strike of the surface break, the first-motion data, and the regional trend of the fault plane geometry. For events deeper than 30 km, all five moment tensor elements can

TABLE VII

Izu-Oshima, Japan, earthquake, 1978: moment tensor (units of $10^{20} \text{ Nm} = 10^{27} \text{ dyne} \cdot \text{cm}$) ($d = 16 \text{ km}$)

Constrained solution ($M_{xz} = M_{yz} = 0$)
$M_{xy} = 0.0845 \pm 0.0125$
$M_{yy} - M_{xx} = 0.0120 \pm 0.0238$
$M_{yy} + M_{xx} = 0.0208 \pm 0.0099$

be determined. Whether the method works well or not depends largely on the quality of the data (e.g. signal-to-noise ratio, calibration, timing accuracy). The IDA records used here are very well calibrated and proved to be extremely useful for mechanism studies.

The method can be implemented on a very small computer. When the IDA data are used (sampling interval of 20 s), the record to be analysed usually consists of only 128–256 data points. Once the spectra are obtained, the remaining computations can be made by using the tables of the excitation functions given in the Appendix and the standard least-squares and eigenvalue routines.

Although the solution obtained by the constrained inversion ($M_{xz} = M_{yz} = 0$) may be too restrictive (either 45° dip slip or vertical strike slip) for detailed studies, it is useful for real-time tsunami warning purposes. For these purposes, the fault type (dip slip or strike slip) and the seismic moment are most important. The constrained solution provides sufficiently accurate information on both of these as shown by Figs. 4, 6 and 12.

As discussed earlier, the dip angle cannot be determined very accurately for a shallow dip slip earthquake. Since the observed amplitude is approximately proportional to $M_0 \sin 2\delta$, the uncertainty in δ results in uncertainty in M_0 . However, the product $M_0 \sin 2\delta$ can be constrained better by the data. Since the vertical component of the fault

displacement is primarily responsible for tsunami generation, this product is probably more useful than the seismic moment itself for tsunami warning purposes.

Acknowledgement

The IDA data used in this study were made available by courtesy of the IDA project team at the Institute of Geophysics and Planetary Physics, University of California, San Diego. We thank Freeman Gilbert, Jon Berger, Duncan Agnew, Guy Masters, Paul Silver and other staff members of the project team for providing valuable information on the instrument calibration and programs for reading and editing the IDA data.

This work was supported by Earth Sciences Section, National Science Foundation Grant No. EAR 78-11973, and U.S. Geological Survey Contract No. 14-08-0001-19755.

Appendix. Rayleigh and Love wave excitation functions for various periods and depths

The excitation functions are $S_R^{(1)}$, $P_R^{(1)}$, $Q_R^{(1)}$, $P_L^{(1)}$ and $Q_L^{(1)}$. The depth d indicates the depth (see Table A1) of the point source and d_M the depth of the lower edge of the extended source (see Table A2). The units are $\text{cm s}/10^{27} \text{dyne} \cdot \text{cm}$.

TABLE A1

Rayleigh and Love wave excitation functions for various periods and depths

N	T (s)	$d=9.75$ km			$d=16.0$ km			N	T (s)
		$S_R^{(1)}$	$P_R^{(1)}$	$Q_R^{(1)}$	$S_R^{(1)}$	$P_R^{(1)}$	$Q_R^{(1)}$		
19	360.00	1.94775	0.96820	-0.01220	1.83101	0.93984	-0.01324	19	360.00
22	324.93	2.31963	1.17628	-0.01121	2.16276	1.13502	-0.01790	22	324.93
25	297.39	2.64175	1.36819	-0.02571	2.44634	1.31255	-0.03551	25	297.39
28	274.80	2.93390	1.54517	-0.03664	2.69799	1.47402	-0.05205	28	274.80
31	255.69	3.18913	1.70406	-0.04469	2.91318	1.61696	-0.06755	31	255.69
34	239.22	3.40400	1.84315	-0.06274	3.08980	1.73990	-0.09120	34	239.22
37	224.78	3.60054	1.97071	-0.07584	3.24748	1.85107	-0.11202	37	224.78
40	211.99	3.76740	2.08318	-0.09220	3.37722	1.94721	-0.13567	40	211.99
43	200.56	3.73941	2.08016	-0.12637	3.32004	1.92750	-0.17929	43	200.56
46	190.29	3.87858	2.17668	-0.14498	3.42444	2.00819	-0.20526	46	190.29

TABLE A1 (continued)

N	T (s)	d=33.0 km			d=43.0 km			N	T (s)
		$S_R^{(1)}$	$P_R^{(1)}$	$Q_R^{(1)}$	$S_R^{(1)}$	$P_R^{(1)}$	$Q_R^{(1)}$		
19	360.00	1.61222	0.86309	-0.07069	1.51666	0.81922	-0.10430	19	360.00
22	324.93	1.85969	1.02400	-0.10472	1.72209	0.96105	-0.15415	22	324.93
25	297.39	2.05526	1.16315	-0.15331	1.87236	1.07909	-0.22033	25	297.39
28	274.80	2.21568	1.28381	-0.20505	1.98627	1.17770	-0.29104	28	274.80
31	255.69	2.34041	1.38512	-0.25832	2.06534	1.25684	-0.36375	31	255.69
34	239.22	2.42835	1.46605	-0.31913	2.10857	1.31580	-0.44391	34	239.22
37	224.78	2.49767	1.53495	-0.37927	2.13435	1.36300	-0.52344	37	224.78
40	211.99	2.54222	1.58943	-0.44178	2.13730	1.39648	-0.60474	40	211.99
43	200.56	2.40340	1.52273	-0.51926	1.94047	1.30028	-0.71180	43	200.56
46	190.29	2.42679	1.56265	-0.58351	1.92324	1.31929	-0.79571	46	190.29
N	T (s)	d=53.0 km			d=62.0 km			N	T (s)
		$S_R^{(1)}$	$P_R^{(1)}$	$Q_R^{(1)}$	$S_R^{(1)}$	$P_R^{(1)}$	$Q_R^{(1)}$		
19	360.00	1.40785	0.77521	-0.13805	1.30063	0.73686	-0.16952	19	360.00
22	324.93	1.56859	0.89787	-0.20380	1.42113	0.84327	-0.24910	22	324.93
25	297.39	1.67114	0.99477	-0.28780	1.48149	0.92244	-0.34810	25	297.39
28	274.80	1.73630	1.07123	-0.37771	1.50486	0.98062	-0.45357	28	274.80
31	255.69	1.76772	1.12817	-0.47010	1.49639	1.01952	-0.56130	31	255.69
34	239.22	1.76455	1.16507	-0.56996	1.45534	1.03885	-0.67587	34	239.22
37	224.78	1.74521	1.19054	-0.66922	1.40020	1.04729	-0.78923	37	224.78
40	211.99	1.70525	1.20291	-0.76969	1.32702	1.04345	-0.90276	40	211.99
43	200.56	1.47529	1.08884	-0.89030	1.05596	0.90770	-1.04323	43	200.56
46	190.29	1.42109	1.08910	-0.99056	0.97160	0.89275	-1.15591	46	190.29
N	T (s)	d=71.0 km			d=108.5 km			N	T (s)
		$S_R^{(1)}$	$P_R^{(1)}$	$Q_R^{(1)}$	$S_R^{(1)}$	$P_R^{(1)}$	$Q_R^{(1)}$		
19	360.00	1.29044	0.69840	-0.21424	0.86252	0.55038	-0.35934	19	360.00
22	324.93	1.38254	0.78850	-0.31379	0.79577	0.58177	-0.52081	22	324.93
25	297.39	1.40929	0.84991	-0.43533	0.66113	0.58162	-0.70837	25	297.39
28	274.80	1.39632	0.88979	-0.56433	0.49373	0.56052	-0.90308	28	274.80
31	255.69	1.35106	0.91060	-0.69549	0.30764	0.52379	-1.09600	31	255.69
34	239.22	1.27296	0.91228	-0.83329	0.10233	0.47216	-1.29081	34	239.22
37	224.78	1.18147	0.90363	-0.96917	-0.10323	0.41434	-1.47833	37	224.78
40	211.99	1.07321	0.88355	-1.10408	-0.31052	0.35040	-1.65846	40	211.99
43	200.56	0.76560	0.73499	-1.25918	-0.73442	0.14917	-1.87947	43	200.56
46	190.29	0.65153	0.70617	-1.38941	-0.92451	0.08480	-2.04415	46	190.29
N	T (s)	d=71.0 km			d=108.5 km			N	T (s)
		$S_R^{(1)}$	$P_R^{(1)}$	$Q_R^{(1)}$	$S_R^{(1)}$	$P_R^{(1)}$	$Q_R^{(1)}$		
19	360.00	0.36521	0.41262	-0.48826	0.10597	0.29105	-0.61650	19	360.00
22	324.93	0.14745	0.39310	-0.69905	-0.20963	0.23188	-0.86994	22	324.93
25	297.39	-0.13097	0.34159	-0.93499	-0.57872	0.14317	-1.14369	25	297.39
28	274.80	-0.42705	0.27172	-1.17363	-0.95255	0.04077	-1.41222	28	274.80
31	255.69	-0.72180	0.19112	-1.40326	-1.30824	-0.06615	-1.66198	31	255.69
34	239.22	-1.01684	0.10109	-1.62704	-1.64787	-0.17617	-1.89609	34	239.22
37	224.78	-1.29542	0.00992	-1.83624	-1.95673	-0.28185	-2.10692	37	224.78
40	211.99	-1.55820	-0.08160	-2.02979	-2.23551	-0.38228	-2.29361	40	211.99
43	200.56	-1.99515	-0.29730	-2.26110	-2.70056	-0.60286	-2.52414	43	200.56
46	190.29	-2.21034	-0.37802	-2.42338	-2.90990	-0.68375	-2.66560	46	190.29

N	T (s)	$d=271.0$ km			$d=371.0$ km			N	T (s)
		$S_R^{(1)}$	$P_R^{(1)}$	$Q_R^{(1)}$	$S_R^{(1)}$	$P_R^{(1)}$	$Q_R^{(1)}$		
19	360.00	-0.57751	0.06305	-0.85212	-1.20334	-0.11086	-1.06039	19	360.00
22	324.93	-1.04092	-0.05311	-1.15884	-1.70877	-0.24543	-1.37646	22	324.93
25	297.39	-1.51413	-0.18627	-1.46421	-2.16130	-0.37895	-1.65956	25	297.39
28	274.80	-1.94515	-0.31827	-1.74081	-2.51872	-0.49524	-1.88616	28	274.80
31	255.69	-2.31213	-0.43941	-1.97516	-2.77192	-0.58768	-2.04914	31	255.69
34	239.22	-2.62298	-0.54925	-2.17268	-2.94084	-0.65883	-2.15980	34	239.22
37	224.78	-2.87349	-0.64381	-2.33065	-3.03570	-0.70907	-2.22233	37	224.78
40	211.99	-3.06834	-0.72319	-2.45077	-3.06852	-0.74096	-2.24283	40	211.99
43	200.56	-3.36258	-0.88010	-2.59973	-3.12571	-0.81389	-2.27645	43	200.56
46	190.29	-3.45524	-0.92547	-2.65429	-3.06653	-0.81246	-2.23316	46	190.29
N	T (s)	$d=471.0$ km			$d=571.0$ km			N	T (s)
		$S_R^{(1)}$	$P_R^{(1)}$	$Q_R^{(1)}$	$S_R^{(1)}$	$P_R^{(1)}$	$Q_R^{(1)}$		
19	360.00	-1.18376	-0.22561	-0.99596	-1.28216	-0.27932	-1.05295	19	360.00
22	324.93	-1.60017	-0.35386	-1.22660	-1.61393	-0.38407	-1.23132	22	324.93
25	297.39	-1.93388	-0.46573	-1.40429	-1.83977	-0.46370	-1.33765	25	297.39
28	274.80	-2.15876	-0.54943	-1.51924	-1.95144	-0.51214	-1.37411	28	274.80
31	255.69	-2.27783	-0.60273	-1.57467	-1.96467	-0.53141	-1.35374	31	255.69
34	239.22	-2.31660	-0.63139	-1.58552	-1.91037	-0.52925	-1.29658	34	239.22
37	224.78	-2.29265	-0.63943	-1.56121	-1.81031	-0.51133	-1.21579	37	224.78
40	211.99	-2.22136	-0.63119	-1.50979	-1.68088	-0.48247	-1.12059	40	211.99
43	200.56	-2.15653	-0.64194	-1.46018	-1.55150	-0.46291	-1.02809	43	200.56
46	190.29	-2.02815	-0.60970	-1.37550	-1.40018	-0.42166	-0.92489	46	190.29
N	T (s)	$d=671.0$ km			N	T (s)			
		$S_R^{(1)}$	$P_R^{(1)}$	$Q_R^{(1)}$					
19	360.00	-1.13036	-0.27869	-0.95596	19	360.00			
22	324.93	-1.33978	-0.34659	-1.06863	22	324.93			
25	297.39	-1.44578	-0.38685	-1.10865	25	297.39			
28	274.80	-1.45729	-0.39977	-1.08754	28	274.80			
31	255.69	-1.39763	-0.39087	-1.02314	31	255.69			
34	239.22	-1.29654	-0.36833	-0.93572	34	239.22			
37	224.78	-1.17367	-0.33778	-0.83799	37	224.78			
40	211.99	-1.04188	-0.30315	-0.73781	40	211.99			
43	200.56	-0.91539	-0.27483	-0.64366	43	200.56			
46	190.29	-0.79095	-0.23893	-0.55344	46	190.29			

TABLE A1 (continued)

N	T (s)	d=9.75 km		d=16.0 km		d=33.0km		N	T (s)
		$P_L^{(1)}$	$Q_L^{(1)}$	$P_L^{(1)}$	$Q_L^{(1)}$	$P_L^{(1)}$	$Q_L^{(1)}$		
19	373.95	-2.65478	-0.06101	-2.65306	-0.08781	-2.64840	-0.11643	19	373.95
22	332.24	-2.84729	-0.06839	-2.84505	-0.09843	-2.83919	-0.12458	22	332.24
25	299.16	-2.99909	-0.07508	-2.99633	-0.10803	-2.98920	-0.13070	25	299.16
28	272.21	-3.10921	-0.08096	-3.10584	-0.11649	-3.09743	-0.13490	28	272.21
31	249.77	-3.19577	-0.08644	-3.19182	-0.12436	-3.18215	-0.13809	31	249.77
34	230.78	-3.26105	-0.09154	-3.25645	-0.13167	-3.24551	-0.14042	34	230.78
37	214.48	-3.31028	-0.09633	-3.30506	-0.13855	-3.29278	-0.14215	37	214.48
40	200.35	-3.34721	-0.10089	-3.34124	-0.14510	-3.32763	-0.14345	40	200.35
43	187.96	-3.37433	-0.10527	-3.36763	-0.15137	-3.35268	-0.14443	43	187.96
46	177.01	-3.39341	-0.10948	-3.38602	-0.15740	-3.36966	-0.14518	46	177.01
N	T (s)	d=43.0 km		d=53.0 km		d=62.0 km		N	T (s)
		$P_L^{(1)}$	$Q_L^{(1)}$	$P_L^{(1)}$	$Q_L^{(1)}$	$P_L^{(1)}$	$Q_L^{(1)}$		
19	373.95	-2.64451	-0.14412	-2.63976	-0.17280	-2.63470	-0.20004	19	373.95
22	332.24	-2.83441	-0.15220	-2.82863	-0.18084	-2.82252	-0.20805	22	332.24
25	299.16	-2.98356	-0.15752	-2.97677	-0.18538	-2.96970	-0.21189	25	299.16
28	272.21	-3.09101	-0.16034	-3.08329	-0.18683	-3.07533	-0.21206	28	272.21
31	249.77	-3.17484	-0.16182	-3.16625	-0.18661	-3.15747	-0.21025	31	249.77
34	230.78	-3.21743	-0.16221	-3.22810	-0.18504	-3.21865	-0.20687	34	230.78
37	214.48	-3.28402	-0.16184	-3.27389	-0.18256	-3.26376	-0.20241	37	214.48
40	200.35	-3.31812	-0.16095	-3.30731	-0.17945	-3.29668	-0.19725	40	200.35
43	187.96	-3.34241	-0.15968	-3.33103	-0.17591	-3.31964	-0.19158	43	187.96
46	177.01	-3.35884	-0.15814	-3.34669	-0.17207	-3.33508	-0.18560	46	177.01
N	T (s)	d=71.0 km		d=108.5 km		d=146.0 km		N	T (s)
		$P_L^{(1)}$	$Q_L^{(1)}$	$P_L^{(1)}$	$Q_L^{(1)}$	$P_L^{(1)}$	$Q_L^{(1)}$		
19	373.95	-2.62890	-0.24205	-2.58915	-0.44160	-2.52844	-0.62900	19	373.95
22	332.24	-2.81554	-0.25052	-2.76762	-0.46154	-2.69401	-0.65892	22	332.24
25	299.16	-2.96170	-0.25380	-2.90607	-0.47254	-2.82035	-0.67634	25	299.16
28	272.21	-3.06639	-0.25256	-3.00392	-0.47563	-2.90712	-0.68268	28	272.21
31	249.77	-3.14770	-0.24888	-3.07909	-0.47445	-2.97189	-0.68305	31	249.77
34	230.78	-3.20808	-0.24327	-3.13385	-0.46989	-3.01721	-0.67869	34	230.78
37	214.48	-3.25255	-0.23638	-3.17332	-0.46298	-3.04788	-0.67104	37	214.48
40	200.35	-3.28494	-0.22862	-3.20122	-0.45452	-3.06792	-0.66117	40	200.35
43	187.96	-3.30759	-0.22028	-3.21987	-0.44495	-3.07926	-0.64982	43	187.96
46	177.01	-3.32241	-0.21157	-3.23135	-0.43465	-3.08380	-0.63740	46	177.01
N	T (s)	d=183.5 km		d=271.0 km		d=371.0 km		N	T (s)
		$P_L^{(1)}$	$Q_L^{(1)}$	$P_L^{(1)}$	$Q_L^{(1)}$	$P_L^{(1)}$	$Q_L^{(1)}$		
19	373.95	-2.44509	-0.81464	-2.17924	-1.07172	-1.82907	-1.17836	19	373.95
22	332.24	-2.59281	-0.85437	-2.27059	-1.11730	-1.85256	-1.20105	22	332.24
25	299.16	-2.70218	-0.87815	-2.32644	-1.14188	-1.84634	-1.20001	25	299.16
28	272.21	-2.77338	-0.88773	-2.34863	-1.14801	-1.81393	-1.17952	28	272.21
31	249.77	-2.82363	-0.88980	-2.35287	-1.14460	-1.76920	-1.14973	31	249.77
34	230.78	-2.85543	-0.88577	-2.34211	-1.13359	-1.71502	-1.11329	34	230.78
37	214.48	-2.87362	-0.87757	-2.32088	-1.11755	-1.65529	-1.07311	37	214.48
40	200.35	-2.88185	-0.86659	-2.29250	-1.09829	-1.59297	-1.03122	40	200.35
43	187.96	-2.88240	-0.85366	-2.25900	-1.07686	-1.52947	-0.98867	43	187.96
46	177.01	-2.87712	-0.83944	-2.22182	-1.05416	-1.46612	-0.94634	46	177.01

TABLE A2

The excitation functions for various d_m

N	T (s)	$d=471.0$ km		$d=571.0$ km		$d=671.0$ km		N	T (s)
		$P_L^{(1)}$	$Q_L^{(1)}$	$P_L^{(1)}$	$Q_L^{(1)}$	$P_L^{(1)}$	$Q_L^{(1)}$		
19	373.95	-1.50466	-0.94122	-1.21111	-0.86453	-0.94700	-0.68984	19	373.95
22	332.24	-1.47510	-0.92954	-1.14498	-0.82569	-0.85737	-0.63776	22	332.24
25	299.16	-1.42384	-0.89981	-1.06668	-0.77276	-0.76551	-0.57768	25	299.16
28	272.21	-1.35538	-0.85685	-0.98071	-0.71121	-0.67507	-0.51454	28	272.21
31	249.77	-1.28117	-0.80914	-0.89596	-0.64901	-0.59190	-0.45433	31	249.77
34	230.78	-1.20386	-0.75911	-0.81408	-0.58821	-0.51648	-0.39836	34	230.78
37	214.48	-1.12651	-0.70897	-0.73688	-0.53070	-0.44921	-0.34761	37	214.48
40	200.35	-1.05102	-0.66019	-0.66521	-0.47729	-0.38983	-0.30234	40	200.35
43	187.96	-0.97837	-0.61343	-0.59931	-0.42828	-0.33777	-0.26232	43	187.96
46	177.01	-0.90927	-0.56918	-0.53916	-0.38372	-0.29236	-0.22721	46	177.01

N	T (s)	$d_M=24.5$ km			$d_M=38.0$ km			N	T (s)
		$S_R^{(1)}$	$P_R^{(1)}$	$Q_R^{(1)}$	$S_R^{(1)}$	$P_R^{(1)}$	$Q_R^{(1)}$		
19	360.00	1.88277	0.95241	-0.01278	1.75525	0.91031	-0.04007	19	360.00
22	324.93	2.23231	1.15331	-0.01493	2.05668	1.09236	-0.05725	22	324.93
25	297.39	2.53297	1.33722	-0.03117	2.30782	1.25518	-0.08874	25	297.39
28	274.80	2.80258	1.50556	-0.04522	2.52596	1.40105	-0.12055	28	274.80
31	255.69	3.03552	1.65558	-0.05742	2.70790	1.52810	-0.15211	31	255.69
34	239.22	3.22910	1.78568	-0.07858	2.85169	1.63503	-0.19196	34	239.22
37	224.78	3.40401	1.90411	-0.09598	2.97683	1.73012	-0.22950	37	224.78
40	211.99	3.55021	2.00749	-0.11640	3.07512	1.81045	-0.26976	40	211.99
43	200.56	3.50597	1.99518	-0.15583	2.98630	1.77250	-0.32712	43	200.56
46	190.29	3.62578	2.08289	-0.17853	3.06067	1.83769	-0.36941	46	190.29

N	T (s)	$d_M=48.0$ km			$d_M=57.5$ km			N	T (s)
		$S_R^{(1)}$	$P_R^{(1)}$	$Q_R^{(1)}$	$S_R^{(1)}$	$P_R^{(1)}$	$Q_R^{(1)}$		
19	360.00	1.69298	0.88654	-0.05684	1.63582	0.86422	-0.07312	19	360.00
22	324.93	1.96935	1.05809	-0.08254	1.88901	1.02597	-0.10685	22	324.93
25	297.39	2.19416	1.20922	-0.12308	2.08931	1.16623	-0.15610	25	297.39
28	274.80	2.38510	1.34275	-0.16505	2.25504	1.28832	-0.20768	28	274.80
31	255.69	2.54019	1.45730	-0.20735	2.38534	1.39132	-0.26002	31	255.69
34	239.22	2.65773	1.55171	-0.25772	2.47868	1.47420	-0.32031	34	239.22
37	224.78	2.75694	1.63430	-0.30622	2.55412	1.54534	-0.37899	37	224.78
40	211.99	2.83034	1.70240	-0.35719	2.60480	1.60227	-0.43988	40	211.99
43	200.56	2.71334	1.64925	-0.42752	2.46515	1.53691	-0.52029	43	200.56
46	190.29	2.76380	1.70238	-0.48068	2.49463	1.57944	-0.58289	46	190.29

N	T (s)	$d_M=66.5$ km			$d_M=89.75$ km			N	T (s)
		$S_R^{(1)}$	$P_R^{(1)}$	$Q_R^{(1)}$	$S_R^{(1)}$	$P_R^{(1)}$	$Q_R^{(1)}$		
19	360.00	1.58186	0.84372	-0.08864	1.50009	0.80294	-0.12388	19	360.00
22	324.93	1.81370	0.99656	-0.12975	1.69272	0.93818	-0.18139	22	324.93
25	297.39	1.99147	1.12698	-0.18701	1.82811	1.04924	-0.25669	25	297.39
28	274.80	2.13428	1.23879	-0.24726	1.92721	1.14086	-0.33623	28	274.80
31	255.69	2.24224	1.33147	-0.30852	1.99218	1.21338	-0.41710	31	255.69
34	239.22	2.31395	1.40412	-0.37755	2.02185	1.26611	-0.50543	34	239.22
37	224.78	2.36838	1.46517	-0.44503	2.03533	1.30760	-0.59210	37	224.78
40	211.99	2.39912	1.51232	-0.51439	2.02707	1.33589	-0.67986	40	211.99
43	200.56	2.23831	1.43562	-0.60447	1.82507	1.23903	-0.78818	43	200.56
46	190.29	2.24947	1.46890	-0.67513	1.80109	1.25488	-0.87555	46	190.29

TABLE A2 (continued)

N	T (s)	$d_M = 24.5$ km		$d_M = 38.0$		$d_M = 48.0$		N	T (s)
		$P_L^{(1)}$	$Q_L^{(1)}$	$P_L^{(1)}$	$Q_L^{(1)}$	$P_L^{(1)}$	$Q_L^{(1)}$		
19	373.95	-2.65382	-0.07593	-2.65127	-0.09502	-2.64951	-0.10783	19	373.95
22	332.24	-2.84604	-0.08511	-2.84281	-0.10371	-2.84062	-0.11637	22	332.24
25	299.16	-2.99755	-0.09342	-2.99362	-0.11099	-2.99099	-0.12314	25	299.16
28	272.21	-3.10734	-0.10074	-3.10267	-0.11684	-3.09963	-0.12819	28	272.21
31	249.77	-3.19357	-0.10755	-3.18819	-0.12194	-3.18471	-0.13235	31	249.77
34	230.78	-3.25849	-0.11388	-3.25237	-0.12639	-3.24847	-0.13574	34	230.78
37	214.48	-3.30738	-0.11983	-3.30050	-0.13035	-3.29620	-0.13857	37	214.48
40	200.35	-3.34389	-0.12550	-3.33623	-0.13396	-3.33150	-0.14100	40	200.35
43	187.96	-3.37060	-0.13093	-3.36216	-0.13729	-3.35700	-0.14314	43	187.96
46	177.01	-3.38930	-0.13615	-3.38004	-0.14041	-3.37451	-0.14504	46	177.01
N	T (s)	$d_M = 57.5$ km		$d_M = 66.5$ km		$d_M = 89.75$ km		N	T (s)
		$P_L^{(1)}$	$Q_L^{(1)}$	$P_L^{(1)}$	$Q_L^{(1)}$	$P_L^{(1)}$	$Q_L^{(1)}$		
19	373.95	-2.64755	-0.12086	-2.64548	-0.13360	-2.64083	-0.16403	19	373.95
22	332.24	-2.83822	-0.12929	-2.83569	-0.14197	-2.83004	-0.17243	22	332.24
25	299.16	-2.98814	-0.13561	-2.98517	-0.14789	-2.97859	-0.17761	25	299.16
28	272.21	-3.09635	-0.13995	-3.09297	-0.15156	-3.08551	-0.17990	28	272.21
31	249.77	-3.18101	-0.14323	-3.17722	-0.15402	-3.16894	-0.18064	31	249.77
34	230.78	-3.24439	-0.14562	-3.24025	-0.15548	-3.23122	-0.18011	34	230.78
37	214.48	-3.29173	-0.14739	-3.28723	-0.15625	-3.27750	-0.17873	37	214.48
40	200.35	-3.32665	-0.14871	-3.32183	-0.15652	-3.31148	-0.17675	40	200.35
43	187.96	-3.35180	-0.14971	-3.34662	-0.15645	-3.33567	-0.17436	43	187.96
46	177.01	-3.36893	-0.15046	-3.36348	-0.15611	-3.35196	-0.17167	46	177.01

References

- Agnew, D., Berger, J., Buland, R., Farrell, W. and Gilbert, F., 1976. International deployment of accelerometers: A network for very long period seismology. *EOS*, 57: 180-188.
- Aki, K., 1966. Generation and propagation of G waves from the Niigata earthquake of June 16, 1964. Part 2. Estimation of earthquake moment, from the G wave spectrum. *Bull. Earthquake Res. Inst., Tokyo Univ.*, 44: 73-88.
- Aki, K. and Richards, P.G., 1980. *Quantitative Seismology, Theory and Methods*, Vol. 1. Freeman, San Francisco, CA, 557 pp.
- Ben-Menahem, A., 1961. Radiation of seismic surface waves from finite moving sources. *Bull. Seismol. Soc. Am.*, 51: 401-435.
- Ben-Menahem, A. and Harkrider, D.G., 1964. Radiation patterns of seismic surface waves from buried dipolar point sources in a flat stratified Earth. *J. Geophys. Res.*, 69: 2605-2620.
- Ben-Menahem, A., Rosenman, M. and Harkrider, D.G., 1970. Fast evaluation of source parameters from isolated surface wave signals. *Bull. Seismol. Soc. Am.*, 60: 1337-1387.
- Boore, D.M., Sims, J.D., Kanamori, H. and Harding, S., 1981. The Montenegro, Yugoslavia, earthquake of April 15, 1979: source orientation and strength. *Phys. Earth Planet. Inter.*, 27: 133-142.
- Dziewonski, A.M. and Gilbert, F., 1974. Temporal variation of the seismic moment tensor and the evidence of precursive compression for two deep earthquakes. *Nature (London)* 247: 185-188.
- Dziewonski, A.M., Chou, T.A. and Woodhouse, J.H., 1980. Determination of earthquake source parameters from waveform data for studies of global and regional seismicity. *J. Geophys. Res.*, 86: 2825-2852.
- Furumoto, M., 1979. Initial phase analysis of R-waves from great earthquakes. *J. Geophys. Res.*, 84: 6867-6874.
- Gilbert, F., 1970. Excitation of the normal modes of the Earth by earthquakes and explosions. *Geophys. J. R. Astron. Soc.*, 22: 223-226.
- Gilbert, F., 1981. An introduction to low-frequency seismology. In: A.M. Dziewonski and E. Boschi, (Editors), *Physics of the Earth's Interior*. North-Holland, Amsterdam, pp. 41-81.
- Gilbert, F. and Buland, R., 1976. An enhanced deconvolution procedure for retrieving the seismic moment tensor from a sparse network. *Geophys. J. R. Astron. Soc.*, 47: 251-255.
- Gilbert, F. and Dziewonski, A.M., 1975. An application of normal mode theory to the retrieval of structural parameters and source mechanisms from seismic spectra. *Philos. Trans. R. Soc. London, Ser. A*, 278: 187-269.
- Harkrider, D.G., 1964. Surface waves in multilayered elastic media. I. *Bull. Seismol. Soc. Am.*, 54: 627-680.
- Haskell, N.A., 1963. Radiation pattern of Rayleigh waves from

- a fault of arbitrary dip and direction of motion in a homogeneous medium. *Bull. Seismol. Soc. Am.*, 53: 619–642.
- Haskell, N.A., 1964. Radiation pattern of surface waves from point sources in a multilayered medium. *Bull. Seismol. Soc. Am.*, 54: 377–393.
- Jarosh, H. and Aboodi, E., 1970. Towards a unified notation of source parameters. *Geophys. J. R. Astron. Soc.*, 21: 513–529.
- Kanamori, H., 1970. Velocity and Q of mantle waves. *Phys. Earth Planet. Inter.*, 2: 259–275.
- Kanamori, H. and Cipar, J.J., 1974. Focal process of the great Chilean earthquake, May 22, 1960. *Phys. Earth Planet. Inter.*, 9: 128–136.
- Kanamori, H. and Stewart, G.S., 1976. Mode of the strain release along the Gibbs fracture zone, Mid-Atlantic ridge. *Phys. Earth Planet. Inter.*, 11: 312–332.
- Knopoff, L., and Randall, J., 1970. The compensated linear vector dipole—a possible mechanism for deep earthquakes. *J. Geophys. Res.*, 75: 4957–4963.
- McCowan, D.W., 1976. Moment tensor representation of surface wave sources. *Geophys. J. R. Astron. Soc.*, 44: 595–599.
- Masters, G. and Gilbert, F., 1979. Source retrieval from a sparse long-period network. *EOS*, 60: 829 (abstract).
- Mendiguren, J.A., 1977. Inversion of surface wave data in source mechanism studies, *J. Geophys. Res.*, 82: 889–894.
- Okal, E.A., 1978. A physical classification of the Earth's spheroidal modes. *J. Phys. Earth*, 26: 75–103.
- Okal, E.A. and Geller, R.J., 1979. On the observability of isotropic seismic sources: the July 31, 1970 Colombian earthquake. *Phys. Earth Planet. Inter.*, 18: 176–196.
- Patton, H., 1980. Reference point method for determining the source and path effects of surface waves. *J. Geophys. Res.*, 85: 821–848.
- Patton, H. and Aki, K., 1979. Bias in the estimate of seismic moment tensor by the linear inversion method. *Geophys. J. R. Astron. Soc.*, 59: 479–495.
- Press, F., 1970. Earth models consistent with geophysical data. *Phys. Earth Planet. Inter.*, 3: 3–22.
- Saito, M., 1967. Excitation of free oscillations and surface waves by a point source in a vertically heterogeneous Earth. *J. Geophys. Res.*, 72: 3689–3699.
- Satô, Y., Usami, T. and Ewing, M., 1962. Basic study on the oscillation of a homogeneous elastic sphere. IV. *Geophys. Mag.*, 31: 237–242.
- Seno, T., Shimazaki, K., Somerville, P., Eguchi, T. and Sudo, K., 1980. Rupture process of the Miyagi-Oki, Japan, earthquake of June 12, 1978. *Phys. Earth Planet. Inter.*, 23: 39–61.
- Shimazaki, K. and Somerville, P., 1979. Static and dynamic parameters of the Izu-Oshima, Japan, earthquake of January 14, 1978. *Bull. Seismol. Soc. Am.*, 69: 1343–1378.
- Tohoku University, 1979. Earthquake off Miyagi prefecture, June 12, 1978. *Rep. Coord. Comm. Earthquake Predict.*, 21: 55–59 (in Japanese).